THE JOURNAL OF PHYSICAL CHEMISTRY C
A JOURNAL OF THE AMERICAN CHEMICAL SOCIETY

pubs.acs.org/JPCC
Article

Exploring the Inner- and Outer-Sphere Mechanistic Pathways of ORR on M−N−Cs with Pyrrolic MN_4 Motifs

Jian Liang Low,* Christina Roth, and Beate Paulus*

Cite This: J. Phys. Chem. C 2024, 128, 5075−5083
Read Online

ABSTRACT: Metal- and nitrogen-doped carbon materials (M−N−Cs) have emerged as promising alternatives to costly platinum-group metals (PGMs) for the oxygen reduction reaction (ORR) in renewable energy applications. Notably, there is increasing experimental and theoretical evidence supporting pyrrolic MN_4 coordination over pyridinic MN_4 in these materials, which aligns closer to the MN_4 geometries found in nature. This study utilizes density functional theory (DFT) to elucidate the ability of each metal to catalyze various ORR mechanisms at the pyrrolic MN_4 sites. Among the M−N−Cs of first−row transition metals, pyrrolic CrN_4 and FeN_4 exhibit exceptional 4e-ORR activity, promoting both inner- and outer-sphere mechanisms and H_2O_2 dissociation. Pyrrolic CoN_4 is also promising for 2e-ORR catalysis due to its effective outer-sphere electron-transfer capabilities. These findings offer valuable insights for designing sustainable electrocatalysts to exploit the full potential of renewable energy sources, advancing the path toward carbon neutrality.

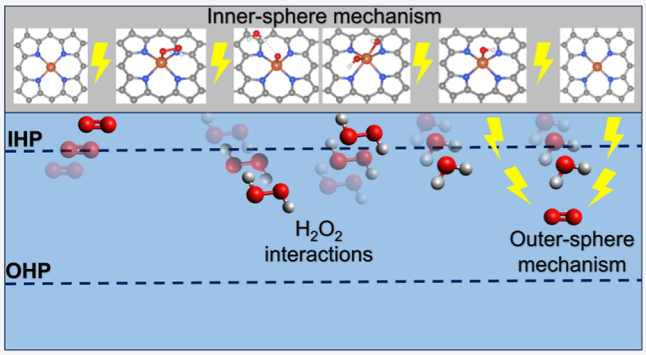

INTRODUCTION

With rapidly growing economic and political pressure toward carbon neutrality, there is a crucial need to develop efficient energy storage and conversion technologies in order to exploit the full potential of renewable energy sources. While fuel cells and metal−air batteries are gaining relevance in relatively large-scale energy applications due to their exceptional energy densities, they often face challenges related to energy conversion efficiency.[1,2] In general, the bottleneck for the energy conversion efficiency of fuel cells and metal-air batteries is the sluggish kinetics of the oxygen reduction reaction (ORR) at the cathode, prompting the need for electrocatalysis.[1,3] The state-of-the-art electrocatalysts for ORR are largely derived from scarce and expensive platinum-group metals (PGMs), severely hampering their economic viability.[4,5] In order to achieve sustainability in the large-scale production and application of such energy storage devices, it is desirable to design alternative electrocatalysts using more naturally abundant elements such as carbon and non-PGMs.[6]

Recently, metal- and nitrogen-doped carbon materials (M−N−Cs) have been widely studied as potential alternatives to PGMs for ORR electrocatalysis, especially with Fe−N−Cs and Co−N−Cs exhibiting ORR currents that are comparable to those of PGMs in alkaline medium.[7−10] Less commonly investigated, yet significant to this study, Cr−N−C and Mn−N−Cs have also been shown to offer promising ORR activity.[11−13] Due to the highly complex structures of these amorphous carbon materials, density functional theory (DFT) is a crucial tool for extracting atomic-level insights on the single atom sites.[14] While the specific coordination can vary across different materials, there is a general consensus that the nature-inspired MN_4 sites are responsible for the observed electrochemical activities.[7] For the modeling of the MN_4 sites, most studies assume the pyridinic MN_4 coordination embedded in a graphene-like lattice.[7,15−18] However, considering that natural MN_4 complexes exclusively contain pyrrolic coordination, the existence of such a structure in carbon-based materials cannot be trivialized. In fact, several recent studies independently identified the pyrrolic MN_4 coordination as the active site responsible for ORR activity in Fe−N−Cs and Co−N−Cs,[19−22] prompting the need for more detailed studies on such pyrrolic MN_4 motifs. Synthesis strategies targeting the selective formation of pyrrolic MN_4 sites have also been developed, allowing for intrinsic activity comparison across M−N−Cs with different metal dopants.[8,10,23]

Compared to the pyridinic structures, DFT studies on the pyrrolic MN_4 sites are relatively sparse. Conventionally, periodic boundary conditions are still imposed for the modeling of pyrrolic MN_4 motifs, leading to structures with hole defects relatively close to the active site, high dopant

Received: January 15, 2024
Revised: February 27, 2024
Accepted: February 27, 2024
Published: March 13, 2024

https://doi.org/10.1021/acs.jpcc.4c00299
J. Phys. Chem. C 2024, 128, 5075−5083

concentrations, or structures with indications of ring strain.[10,24−26] Furthermore, imposing the periodic boundary conditions often entails several technical challenges, namely, the high computational cost of hybrid functionals and the influence of lattice strain on the reactivity.[27,28] For transition metal complexes, GGA functionals can produce computational artifacts arising from the self-interaction error and the associated delocalization error.[29−31] In addition, Kirchhoff et al. showed that the self-interaction error of GGA and meta-GGA functionals can manifest even on nitrogen-doped graphene without transition metals, further emphasizing the importance of hybrid functionals for carbon-based catalysis.[32] Unfortunately, as pointed out by Di Liberto et al., this nontrivial source of error is frequently ignored or mishandled, possibly leading to exaggerated results with regard to inner-sphere reactivity.[14,28] For periodic calculations where hybrid functionals are less practical due to computational costs, the Hubbard correction (DFT + U) could be invoked to mitigate the self-interaction error through calibration with an intuitively "similar" reference material, but it can still cause issues pertaining the transferability of Hubbard parameters and reproducibility across systems.[28] In the same publication, it was also reported that even with a reliable GGA + U that matched the results from hybrid functionals, the reactivity on periodic systems can be artifacts of suboptimal lattice parameters, which are not typically optimized during the reaction studies. Fortunately, in recent publications, it could be shown that the periodic boundary condition is not really necessary for the description of the chemical properties of the MN_4 site since the intrinsic properties of MN_4 sites are often only dependent on the local chemical environment.[19,21,26,33] Utilizing a cluster model not only makes the construction of the pyrrolic MN_4 structures more achievable but also enables a relatively low-cost implementation of the hybrid functionals in place of the GGA or GGA + U methodologies.

For the discussion of ORR activity and selectivity, it is necessary to distinguish between the two-electron pathway (2e-ORR) in which O_2 is partially reduced to H_2O_2 and the four-electron pathway (4e-ORR) where the complete reduction to H_2O occurs. While there are certain situations where the 2e-ORR is desired for the H_2O_2 synthesis,[22,34,35] the 4e-ORR pathway is generally preferred for energy conversion applications (e.g., fuel cells) as it maximizes the current densities and minimizes harmful side reactions with the corrosive H_2O_2.[36] Even for the overall 4e-ORR selectivity, the mechanism can be further classified into the direct 4e-ORR or indirect pathways where H_2O_2 is produced and consumed as an intermediate.[18] In a selectivity study using the rotating ring disk electrode (RRDE) measurements, Bonakdarpour et al. showed that the macroscopically measured H_2O_2 selectivity is heavily dependent on the catalyst loading, increasing from less than 5% to more than 95% H_2O_2 as the catalyst loading decreases.[37] This implies that even the apparent 4e-ORR selectivity of Fe−N−Cs should be more accurately described as a 2e + 2e or a 2e × 2e process, which cannot really be explained with an inner-sphere mechanism.[7]

Besides the overall selectivity, the potential-dependent rate-limiting steps can be differentiated into an inner-sphere mechanism, in which the electron is transferred directly to a strongly bound adsorbate near the inner Helmholtz plane (IHP), or an outer-sphere mechanism, where the electron is transferred to species near the outer Helmholtz plane (OHP).[35,38,39] In alkaline media, which generally require lower overpotentials, the outer-sphere mechanism gains relevance due to the presence of adsorbed hydroxyl species.[38,40] Therefore, besides the conventional studies of active site−adsorbate interactions corresponding to the inner-sphere mechanism, we further investigated the intrinsic electronic properties of the active site correlating to its outer-sphere electron-transferring capabilities as well as the respective interactions between the active sites with inevitably produced H_2O_2.

COMPUTATIONAL METHOD

All calculations were performed with spin-unrestricted Kohn−Sham DFT using the program package TURBOMOLE.[41] For the modeling of the carbon matrix, we used pyrrolic $MN_4C_{96}H_{24}$ and pyridinic $MN_4C_{98}H_{26}$ clusters terminated by hydrogen atoms. Five- and seven-membered rings were introduced into the pyrrolic clusters to keep the ligand-free structures planar.[26] Excluding the hydrogen atoms, the effective metal concentration is 4.4%$_{wt}$, reasonably close to recently achieved dopant concentrations through the templating-transmetalation techniques.[8,9] We applied the hybrid PBE0 functional[42,43] with Grimme's empirical dispersion correction with the Becke−Johnson damping function (D3(BJ)).[44,45] Geometry optimizations were performed with the def2-SVP basis, while a larger def2-TZVP basis was applied for single-point calculations in combination with the COSMO solvation model.[46,47] Electronic steps were converged to 10^{-7} au in the total energy and 10^{-4} au in the orbital energies, while geometric steps were converged to 10^{-6} au in the total energy and 10^{-3} au in the geometric gradient. Each cluster was calculated with various multiplicities, and the one that gave the lowest energy was chosen for further analysis. Atomic charge and spin populations as well as d-orbital occupations were obtained with the natural population analysis.[48] Atomic structures were visualized with VESTA.[49]

For the calculation of potential-dependent intermediate energies for ORR, we applied the computational hydrogen electrode from which the free energy of a proton and electron is defined by

$$G_{H^+ + e^-} = \frac{1}{2}G_{H_2} - eU \tag{1}$$

where U is the applied potential relative to the reversible hydrogen electrode (RHE).[50] The free energies of gaseous species (H_2 and O_2) were calculated from their DFT energies along with zero-point energies, the enthalpy of a linear ideal gas $\left(\frac{7}{2}kT\right)$, and the tabulated entropies.[51] Due to the complexity of acquiring ab initio thermodynamic state functions for liquids that truly account for their configurational entropy, we extrapolated the free energy of water from the free energy of combustion of H_2.[51]

$$G_{H_2O} = G_{H_2} + \frac{1}{2}G_{O_2} - 2.46\ \text{eV} \tag{2}$$

Finally, in order to obtain the free energy of each cluster from the DFT energies E_{DFT}, we calculated the zero-point energies and Helmholtz energy at temperature T = 298 K from the vibrational frequencies with the harmonic approximation.

https://doi.org/10.1021/acs.jpcc.4c00299
J. Phys. Chem. C 2024, 128, 5075−5083

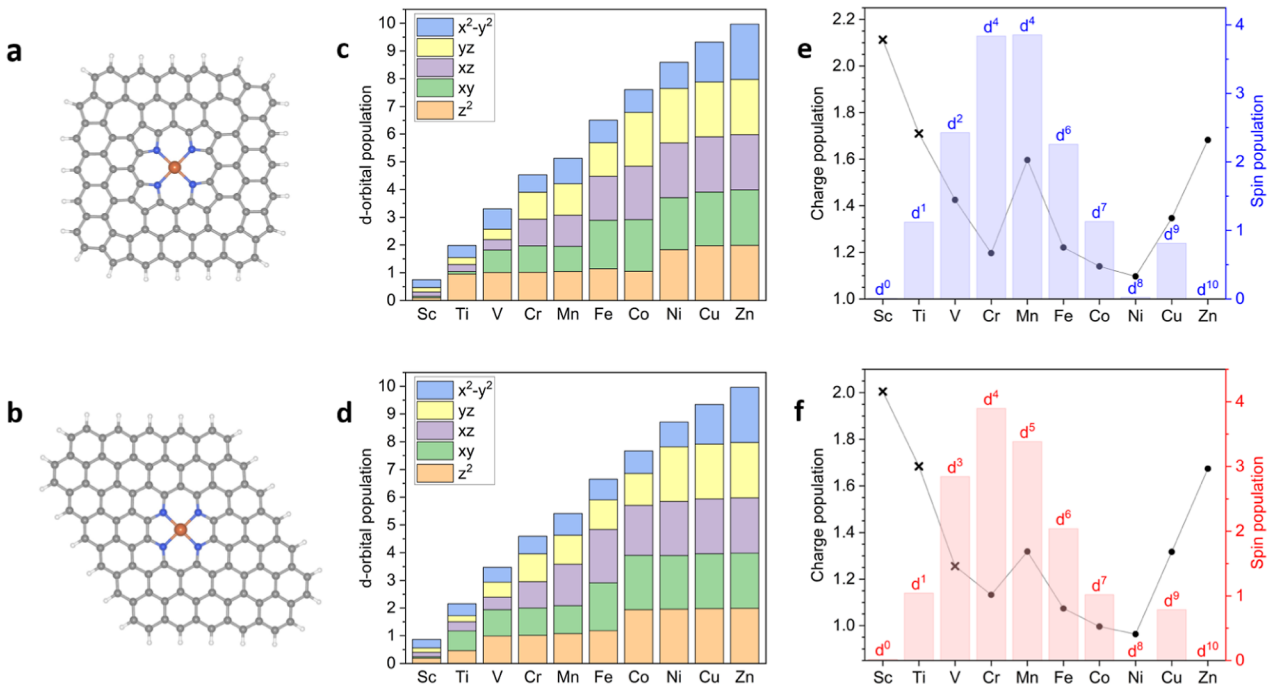

Figure 1. (a,b) Structural model of a planar pyrrolic and pyridinic MN_4 cluster. (c,d) d-Orbital population derived from natural population analysis. (e,f) Charge and spin population of transition metal M in the MN_4 site along with the assigned metal-centered d-orbital configuration. The final electronic structures were obtained with PBE0/def2-TZVP with the COSMO solvation model. Atoms marked with crosses in (e,f) are significantly displaced from the N_4 plane.

$$G_{\text{cluster}} = E_{\text{DFT}} + \sum_i \left[\frac{1}{2} hc\nu_i + k_B T \ln\left(1 - \exp\left(-\frac{hc\nu_i}{k_B T}\right)\right)^{-1} \right] \quad (3)$$

where h is the Planck's constant, c is the speed of light, k_B is the Boltzmann's constant, and ν_i is the wavenumber corresponding to the vibrational frequency of normal mode i.

RESULTS AND DISCUSSION

Electronic Structure of the Ligand-Free MN_4 Sites. For a preliminary understanding of the site-specific ORR activities, we first analyzed the intrinsic electronic structures of ligand-free MN_4 sites. In a previous publication, it was shown that the popular catalytically active metals in the M−N−Cs (M = Fe, Co) tend to participate heavily in covalent interactions with the π-system of the carbon lattice,[26] thereby decreasing their tendency to form pyrrolic MN_4 sites.[8] However, these metals could still be incorporated into pyrrolic sites upon trans-metalation from Zn−N−C and Mg−N−C,[8,52] producing carbon materials with similar overall morphology as well as density and coordination environment of active sites.[23]

For transition metal complexes, the oxidation state of the metal is strongly correlated to its d-orbital occupation and spin population. Figure 1 shows the occupation of the d-orbitals from Sc to Zn and the respective charge and spin populations derived from natural population analysis. The corresponding projected density of states (PDOS) for the d-orbitals is shown in Figure S1. With the exception of Cu and Zn, all transition metals exhibit only fractional occupation of the $d_{x^2-y^2}$ orbital resulting from the σ bonding with N atoms. The strength of the σ bond, as measured by the occupation of the $d_{x^2-y^2}$ orbital, increases with the planarity of the metal binding (Sc < Ti < V) but decreases with the M−N bond length (Fe, Co, Ni > V,Cr) (Geometries in Table S1). As a result of the strong σ-interactions, the antibonding $d_{x^2-y^2}$ only starts to fill for Cu and Zn, accompanied by a sharp decrease in the strength of the M−N_4 binding.[26] Based on the projected PDOS (Figure S1) and the visualization of the d-orbitals of pyrrolic ZnN_4 (Figure S2), we observed that the energy of the antibonding $d_{x^2-y^2}$ is about 6 eV higher than the other metal-centered orbitals, thereby justifying its unfavorable occupation for transition metals in MN_4 sites.

Besides the σ interactions, π-interactions are also highly relevant in these systems, evident in the fractional occupations of the d_{xz} and d_{yz} orbitals for early transition metals (M = Sc, Ti, and V). Due to these π-interactions, the metal-centered antibonding d_{xz} and d_{yz} orbitals can be destabilized relative to other orbitals, leading to deviations in the order of orbital occupations from standard ligand field theory. For example, in pyrrolic NiN_4 where d-orbitals except the antibonding $d_{x^2-y^2}$ are filled (low spin d^8), the d_{xy} orbital is lower in energy than the molecular orbitals with contributions from the d_{xz} and d_{yz} orbitals (Figure S3).

Neglecting the fractional occupations arising from the ligand-centered σ and π orbitals, we can determine the oxidation state of each transition metal from the d-orbital occupation and spin. The first transition metals (Sc, Ti, and V) prefer the oxidation state of +III, largely consistent with the tendency of early transition metals toward higher oxidation states due to lower electronegativities. In contrast, late transition metals (M = Fe, Co, Ni, Cu, and Zn) with higher electronegativities have clear preferences for the +II oxidation state, in line with the desired oxidation state for the N_4 site.

https://doi.org/10.1021/acs.jpcc.4c00299
J. Phys. Chem. C 2024, 128, 5075−5083

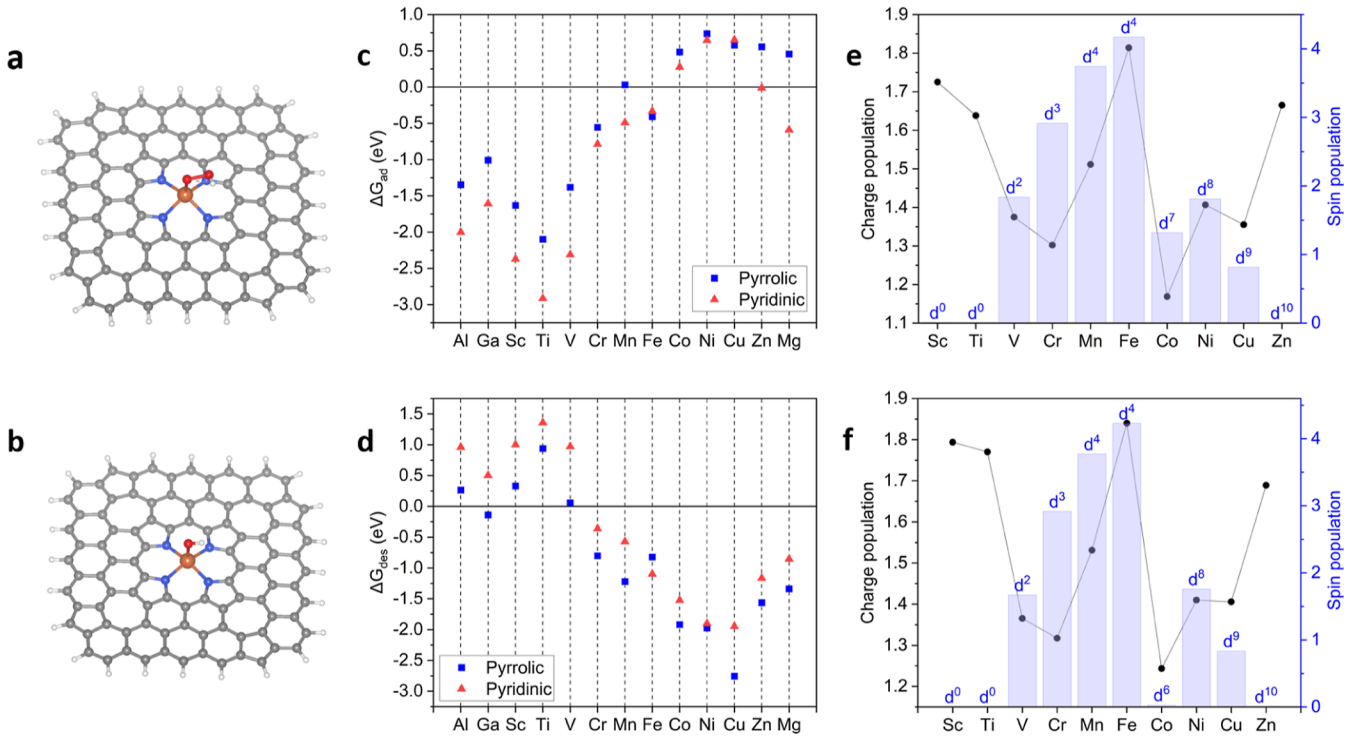

Figure 2. Structural model of pyrrolic (a) *OOH and (b) *OH clusters. Free energy of potential-dependent (c) adsorption step ΔG_{ad} and (d) desorption step ΔG_{des} at 0 V_{RHE}. Charge and spin population of transition metal M in the pyrrolic (e) *OOH and (b) *OH sites along with the assigned metal-centered d-orbital configuration. The final electronic structures were obtained with PBE0/def2-TZVP with the COSMO solvation model.

Cr(II) and Mn(III) are notable outliers in the series, each possessing a different oxidation state from their adjacent metals but share a common high spin d^4 configuration. Considering the high energy of the antibonding $d_{x^2-y^2}$ orbital, the most plausible reason for the anomalies in Cr and Mn is the "half-filled" occupation of the stable d-orbitals in a square-planar complex. For Mn, the occupation of the $d_{x^2-y^2}$ is marginally higher than that for Cr along with a much higher charge population, indicating that it is indeed more favorable for Mn to lose the additional electron, thereby being oxidized to +III, than to fully occupy the antibonding $d_{x^2-y^2}$ orbital or undergo spin pairing.

For a brief comparison of the electronic structure between the pyrrolic and pyridinic MN_4 motifs in Figure 1, we observed that most transition metals exhibit similar charge and spin populations in either MN_4 cluster. In general, the stronger covalent interactions in pyridinic sites lead to smaller charge populations of the metal atoms in the pyridinic clusters. The most significant differences between the pyrrolic and pyridinic clusters are observed in VN_4 and MnN_4 as the increased d-orbital populations bring the respective metal closer to the +II oxidation state. For MnN_4, the anomalous high-spin d^4 configuration appears to be less favored in the pyridinic motif, evident in the partial spin pairing leading to a higher occupation of the d_{xz} orbital.

Inner-Sphere Mechanism. For an inner-sphere ORR mechanism, the most commonly proposed mechanism is the associative mechanism with stepwise protonation of the adsorbed O_2 molecule.

$$\text{free} + O_2 + (H^+ + e^-) \rightarrow {}^*OOH \quad (4)$$

$$^*OOH + (H^+ + e^-) \rightarrow {}^*O + H_2O \quad (5)$$

$$^*O + (H^+ + e^-) \rightarrow {}^*OH \quad (6)$$

$$^*OH + (H^+ + e^-) \rightarrow \text{free} + H_2O \quad (7)$$

The first and last reaction steps are of particular importance for the inner-sphere ORR activity, as they correspond to the potential dependent adsorption and desorption steps in the ORR cycle. We thus studied the free energies of reductive adsorption to *OOH (ΔG_{ad}) and the reductive desorption from *OH (ΔG_{des}), corresponding to the processes in eqs 4 and 7, respectively

$$\Delta G_{ad} = G_{^*OOH} - G_{free} - G_{O_2} - G_{H^+ + e^-} \quad (8)$$

$$\Delta G_{des} = G_{free} + G_{H_2O} - G_{^*OH} - G_{H^+ + e^-} \quad (9)$$

According to Sabatier's principle and its applications in electrocatalysis,[53,54] an ideal ORR catalyst should bind strongly to OOH such that molecular oxygen could be activated but weakly enough to OH to prevent irreversible oxidation of the active site. Thus, both the adsorption (ΔG_{ad}) and desorption (ΔG_{des}) steps should be as exergonic as possible. However, due to similarities in the metal−ligand interactions, ΔG_{ad} is negatively correlated to ΔG_{des}, as depicted in the scaling relation shown in Figure S5. Therefore, in accordance with Sabatier's principle, MN_4 sites with intermediate reactivities should be employed for ORR catalysis assuming an inner-sphere mechanism.

Looking closely into the ΔG_{ad} and ΔG_{des} of the individual metals shown in Figure 2d,e and the resulting free−energy diagrams for ORR on pyrrolic MN_4 motifs in Figure S4a−c, we could identify potential metal dopants for promoting ORR

https://doi.org/10.1021/acs.jpcc.4c00299
J. Phys. Chem. C 2024, 128, 5075−5083

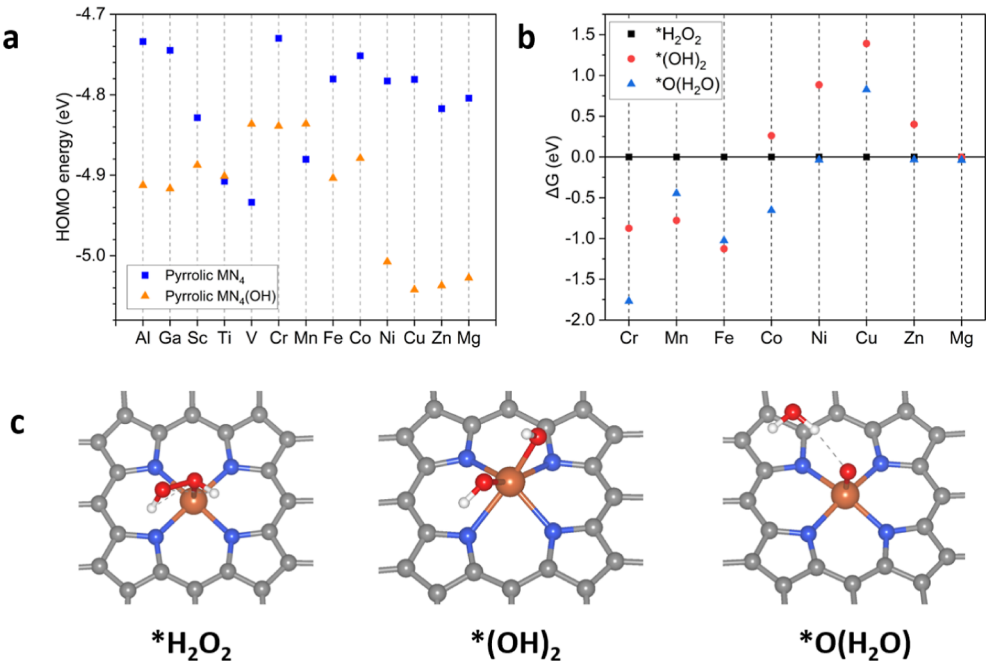

Figure 3. (a) HOMO energy of free and OH-bound pyrrolic motif. (b) Relative free energy between isomeric intermediates $*H_2O_2$ (defined as zero), $*(OH)_2$, and $*O(H_2O)$. (c) Close-up views of three intermediates at the pyrrolic FeN_4 cluster. Geometries were obtained with PBE0/def2-SVP. The final electronic structures were obtained with PBE0/def2-TZVP with the COSMO solvation model.

among the pyrrolic MN_4 sites. The early transition metals (M = Sc, Ti, and V) along with group 13 metals (M = Al and Ga) bind very strongly to both OOH and OH, resulting in highly negative ΔG_{ad} and positive ΔG_{des}. The exceptionally strong binding can be attributed to destabilization of the MN_4 structure as a result of the initial mismatch between the +III metal oxidation state and the ideal −II oxidation state of the N_4 site. Thus, the reductive desorption step on these MN_4 sites is already endergonic even at 0 V_{RHE} (Figure S4b), implying that regeneration of the ligand-free active site is thermodynamically unfavorable at higher ORR potentials. The complete opposite of the metals that bind too strongly to ligands are the late transition metals (M = Co, Ni, Cu, and Zn) and group 2 metal (Mg) where the ΔG_{ad} values are already positive at 0 V_{RHE}. The poor reactivity of these MN_4 sites can be traced to the retention of the +II oxidation state of these metals upon ligand binding, resulting in the formal oxidation of the N_4 site to a less optimal −I oxidation state. Interestingly, for Co, while the binding of OH oxidizes the transition metal to the +III (low spin d^6) oxidation state, the binding of the binding of the OOH does not. For these relatively inert MN_4 sites, an associative inner-sphere mechanism would be unfeasible without external influences to stabilize the *OOH intermediate.

Among the pyrrolic sites, CrN_4 and FeN_4 have the most promising inner-sphere ORR reactivity as both the adsorption (ΔG_{ad}) and desorption steps (ΔG_{des}) are exergonic at 0 V_{RHE}. In the presence of an axial ligand, Cr is generally oxidized from the +II (high spin d^4) to the +III (high spin d^3) oxidation state. Surprisingly, yet familiar, both Mn and Fe adopt the high-spin d^4 configuration in the pyrrolic MN_4 site upon binding of OOH or OH. As the formal oxidation state of Mn remains unchanged, the reactivity of Mn is relatively poor compared to that of Cr and Fe. In contrast, the high charge and spin population of Fe in both the *OOH and *OH intermediates indicate an unusually high +IV oxidation state in order to adopt the d^4 configuration. Similar to Cr, the ability of Fe to adjust its oxidation state to the presence of an axial ligand confers moderate reactivity to the active site, thus making it ideal for promoting the inner-sphere ORR mechanism.

Briefly comparing the reactivities of pyrrolic and pyridinic MN_4 sites (Figures 2c,d and S4), we observed that the pyridinic sites generally exhibit higher inner-sphere reactivity with a more negative ΔG_{ad} and more positive ΔG_{des}. Universally, the stronger binding of ligands implies destabilization of the ligand-free MN_4 sites, consistent with previous findings that such metals often exhibit poor affinity to pyridinic structures.[26] In this regard, modeling the inner-sphere mechanisms on the pyridinic sites may appear to be more promising at the first glance due to the more exergonic first protonation step to *OOH. However, considering the last two data points in Figure 2c, the inner-sphere mechanism on pyridinic sites leads to an erroneous prediction that Zn−N−C and Mg−N−C should be similar, or even higher, in reactivity compared to Fe−N−Cs, contrary to the observed differences in the intrinsic activity between isomorphic Zn−N−Cs and Fe−N−Cs.[23,52] We note that the apparent reactivity of the pyridinic ZnN_4 site is also implied in a recent work by Karmodak et al.,[55] further substantiating the instability of pyridinic ZnN_4. In addition, even for the pyridinic motifs, the apparently high inner-sphere activity of FeN_4 and CoN_4 reported in previous studies[16,56,57] becomes greatly suppressed once hybrid functionals are applied. This effect corroborates well with a study by Barlocco et al., who reported that the PBE functional overestimated the stability of the $H-CoN_4$ intermediate for hydrogen evolution reaction (HER) by 0.5 eV compared to the PBE0 functional, leading to an exaggeration of its theoretical HER activity.[27,28] Despite the partial success of the conventional inner-sphere mechanism in explaining the reactivity of materials like Fe−N−Cs, it cannot fully account for reactivity trends among the late transition metals (M = Co−Zn) or even the reactivity differences

https://doi.org/10.1021/acs.jpcc.4c00299
J. Phys. Chem. C 2024, 128, 5075−5083

between the acidic and the alkaline medium. Therefore, we performed an alternative study in order to determine the possible influence of the outer-sphere mechanism on M−N−Cs, noting that its significance has already been highlighted for metal-based and graphene-based catalysts in the alkaline medium.[38,40,58]

Outer-Sphere Electron Transfer. Although weak interactions with intermediates can be detrimental to the inner-sphere activity, this does not necessarily imply that such M−N−Cs are unsuitable for ORR catalysis. Most notably, Co−N−Cs have been widely shown to exhibit excellent ORR activities, with relatively high 2e-ORR selectivity,[59] despite poor interactions with adsorbates. This somewhat counter-intuitive, Sabatier-defying, ORR activity can be explained by the outer-sphere mechanism, in which a net electron transfer to oxygen in the OHP occurs without direct adsorption.[38] The outer-sphere mechanism is especially significant in alkaline media as the metals' interactions with hydroxides can interfere with the adsorption of intermediates. As observed from ab initio calculations, a descriptor for the ability of M−N−Cs to donate electrons would be the Fermi energy or, in the case of cluster models, the energy of the highest occupied molecular orbital (HOMO).[60,61]

Figure 3a shows the HOMO energies of the ligand-free and OH-bound pyrrolic MN_4 clusters. Among the ligand-free sites, transition metals in the +II oxidation state (M = Cr, Fe, Co, Ni, Cu, and Zn) generally lead to higher HOMO energies compared to those in the +III oxidation state (M = Sc, Ti, V, and Mn). MN_4 sites containing the p-block metals (M = Al and Ga) are outliers to this trend, with the ligand-free sites exhibiting relatively high HOMO energies despite their +III oxidation state. Interestingly, the binding of an OH ligand leads to a reversal in the trend in HOMO energies, with metals in the +III/+IV oxidation state (M = Sc, Ti, V, Cr, Mn, Fe, Co, and Ga) generally producing higher HOMO energies than those in the +II oxidation state (M = Mg, Ni, Cu, and Zn). Considering their relatively high HOMO energies in both the free and ligand bound states, MN_4 sites with M = Al, Ga, Cr, Fe, or Co are expected to have significant contributions from the outer-sphere mechanism regardless of the presence of axial ligands. Especially for Cr and Fe where metal−ligand interactions are moderately strong, both the inner and outer mechanisms can even occur simultaneously, further boosting their already exceptional ORR activities.

Interactions with H_2O_2. Even though the outer-sphere mechanism can, in principle, assist in electron transfer and increase the overall ORR currents, its adsorption-free nature would inevitably lead to the production of H_2O_2. As such, the excellent ability of FeN_4 to promote the outer-sphere mechanism partially contradicts the fact that Fe−N−Cs are known to be highly selective toward 4e-ORR, especially in alkaline media. In order to understand the selectivity toward 2e- or 4e-ORR, it is necessary to investigate the interactions between the produced H_2O_2 with the MN_4 sites. For that purpose, we studied three different isomeric structures shown in Figure 3c in the pyrrolic MN_4 sites, namely, the physisorbed $*H_2O_2$, the dissociated $*(OH)_2$, and the $*O(H_2O)$ structure, which would have been produced following the reduction of the *OOH intermediate (eq 5). Metals that are irreversibly poisoned by OH at typical ORR potentials are excluded (M = Al, Ga, Sc, Ti, and V) as it is unlikely for them to have free MN_4 sites for interaction with H_2O_2 under typical ORR conditions.

Among the remaining metals in pyrrolic MN_4 sites, we further distinguish between metals that are inert toward H_2O_2 from those with at least one stable water-producing intermediate, namely, either $*(OH)_2$ or $*O(H_2O)$ (Figure 3b). Consistent with their universally weak interactions with the adsorbates, MN_4 sites with M = Mg, Ni, Cu, or Zn clearly belong to the former group as the formation of either $*(OH)_2$ or $*O(H_2O)$ from $*H_2O_2$ is determined to be endergonic or reversible at best. It is thus unlikely for these MN_4 sites to be involved in promoting the subsequent H_2O_2 reduction reaction (H_2O_2RR) within the IHP. Meanwhile, metals with intermediate reactivities (M = Cr, Mn, and Fe) favor the formation of both water-producing intermediates due to their abilities to adopt higher oxidation states. In particular, the exergonic formation of the $*(OH)_2$ intermediate implies a significant driving force toward the dissociation of H_2O_2 at these sites. While such an interaction is consistent with the relatively high H_2O_2RR currents measured on Mn−N−Cs and Fe−N−Cs[62] and the generally high 4e-ORR selectivity of the latter, it can have detrimental effects on the stability of these active sites, one of the key limitations reported in Fe−N−C catalysts.[7,63] In particular, if either of the OH fails to bind to the metal upon dissociation of H_2O_2, OH radicals could be produced in a Fenton-like reaction,[64] inducing oxidative stress on the carbon matrix.[63,65−67] Such a process is especially relevant in acidic media where the H_2O_2 remains in its protonated form.[36,68] Therefore, although the complementary outer-sphere mechanism is theoretically favorable for producing higher currents, it could in fact be detrimental to the corrosion resistance of metals such as Cr and Fe in the pyrrolic MN_4 site due to their strong interactions with H_2O_2. In order to increase the long-term stability of such materials, modifications should be targeted at either decreasing the relative contribution of the outer-sphere mechanism (but potentially leading to smaller currents) or minimizing interactions of FeN_4 sites with H_2O_2, for example, by providing alternative active sites for H_2O_2RR that do not produce OH radicals.

Besides Fe−N−Cs, Co−N−Cs are also popular for ORR electrocatalysis, especially toward 2e-ORR. As discussed in the previous section, pyrrolic CoN_4 sites have relatively high HOMO energies to promote electron donation regardless in both the ligand-free and OH-bound forms (Figure 3a). Additionally, due to its transitional position between two strongly contrasting groups of MN_4 sites (M = Cr, Mn, and Fe vs M = Ni, Cu, and Zn), CoN_4 is unique among the studied transition metals in its interactions with H_2O_2. While the direct dissociation of $*H_2O_2$ to form $*(OH)_2$ is endergonic, the formation of the $*O(H_2O)$ intermediate is relatively stable compared to $*H_2O_2$ (Figure 3b). The former suggests that pyrrolic CoN_4 would not be able to catalyze the subsequent reduction of H_2O_2 within the IHP, leading to smaller currents and also lower production of destructive OH radicals compared to the more reactive metals (M = Cr, Mn, and Fe). Nevertheless, the reduction of an adsorbed *OOH intermediate is still thermodynamically more likely to form $*O(H_2O)$ than to form $*H_2O_2$. Therefore, depending on the desired application, external means to promote or suppress interactions with axial ligands for the inner sphere mechanism would be crucial in modulating the overall ORR selectivity of Co−N−Cs.

https://doi.org/10.1021/acs.jpcc.4c00299
J. Phys. Chem. C 2024, 128, 5075−5083

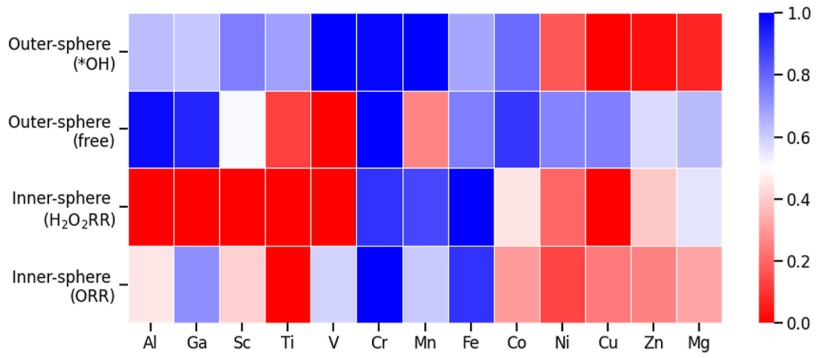

Figure 4. Heatmap illustrating the ratings of various processes based on their respective energies, where a rating of 0 (red) represents the worst performance and a rating of 1 (blue) signifies the best. The processes evaluated include the free energy of the most endergonic step for inner-sphere ORR, the dissociation energy of physisorbed H_2O_2 for H_2O_2RR, and the respective HOMO energies for outer-sphere electron transfer.

CONCLUSIONS

In summary, we performed an extended study of the ORR on M−N−Cs containing first row transition metals as well as group 2 and group 13 metals, taking into consideration not only the conventional inner-sphere mechanism but also the possibility of an outer-sphere mechanism leading to 2e-ORR and 2e + 2e-ORR pathways. An overview of each metal's ability to participate in the inner-sphere and outer-sphere mechanism is depicted in Figure 4.

In general, while the conventional inner-sphere mechanism can qualitatively explain the ORR activity for certain materials like Fe−N−Cs, there are instances where the mechanism contradicts experimental observations, especially the reactivity comparison among M−N−Cs in alkaline media for late transition metals. While all metals can contribute to the outer-sphere mechanisms in their stable form, only those with intermediate reactivities can promote the inner-sphere mechanism and the dissociation of H_2O_2. As a result of the change in metal oxidation state upon the binding of axial ligands, pyrrolic CrN_4 and FeN_4 are exceptional in their ability to promote 4e-ORR as they not only catalyze the inner-sphere mechanism and H_2O_2 dissociation but are also relatively good electron donors regardless of the presence of axial ligands. However, the H_2O_2 produced from an outer-sphere mechanism could be the Achilles' heel to their long-term stability. In contrast, while CoN_4 does not interact as strongly with axial ligands, it is still able to promote the outer-sphere electron transfer in both the ligand-free and OH-adsorbed states, making it suitable for 2e-ORR applications. In addition to showcasing the influence of the oxidation state of metal M on the inner-sphere ORR activity, this study highlights the significance of factoring in contributions from the outer-sphere mechanism as well as interactions with H_2O_2 to justify the overall ORR activity, selectivity, and long-term stability. This insight holds promise in catalyst design, as the targeted manipulation of the preferred electron transfer mechanism and interactions with H_2O_2 could be crucial in mitigating the current limitations of various M−N−C catalysts.

ASSOCIATED CONTENT

Supporting Information

The Supporting Information is available free of charge at https://pubs.acs.org/doi/10.1021/acs.jpcc.4c00299.

DFT energies, vibrational free energy correction terms, and spin states and geometries of ligand-free, *OOH, and *OH structures; projected density of state plots for transition metals; d-orbital analysis for pyrrolic ZnN_4 and NiN_4; scaling relation plot and overall free-energy diagrams for the inner-sphere ORR mechanism; and charge- and spin population of metal M in pyridinic *OOH and *OH (PDF)

DFT-optimized cartesian coordinates (.xyz) of the MN_4 motifs used in this study of MN_4 motifs (ZIP)

AUTHOR INFORMATION

Corresponding Authors

Jian Liang Low − *Institute of Chemistry and Biochemistry, Freie Universität Berlin, Berlin 14195, Germany;* orcid.org/0000-0002-4875-1482; Email: low.jian.liang@fu-berlin.de

Beate Paulus − *Institute of Chemistry and Biochemistry, Freie Universität Berlin, Berlin 14195, Germany*; Phone: +49 (0) 30 838 52051; Email: b.paulus@fu-berlin.de

Author

Christina Roth − *Chair of Electrochemical Process Engineering, Universität Bayreuth, Bayreuth 95447, Germany;* orcid.org/0000-0003-1159-2956

Complete contact information is available at: https://pubs.acs.org/10.1021/acs.jpcc.4c00299

Notes

The authors declare no competing financial interest.

ACKNOWLEDGMENTS

J.L.L. acknowledges the Elsa-Neumann Scholarship for funding and support. The computations were performed with resources provided by the North-German Supercomputing Alliance (HLRN) and computer facilities of the Freie Universität Berlin (ZEDAT). We would like to thank Dr. Tim-Patrick Fellinger (BAM) and Dr. Davide Menga (MIT) for the experimental characterization of the outer-sphere mechanism, which inspired this study. The publication of this article was funded by the Freie Universität Berlin.

REFERENCES

(1) Shao, W.; Yan, R.; Zhou, M.; Ma, L.; Roth, C.; Ma, T.; Cao, S.; Cheng, C.; Yin, B.; Li, S. Carbon-Based Electrodes for Advanced Zinc-Air Batteries: Oxygen-Catalytic Site Regulation and Nanostructure Design. *Electrochem. Energy Rev.* **2023**, *6*, 11.

(2) Ning, F.; He, X.; Shen, Y.; Jin, H.; Li, Q.; Li, D.; Li, S.; Zhan, Y.; Du, Y.; Jiang, J.; et al. Flexible and Lightweight Fuel Cell with High Specific Power Density. *ACS Nano* **2017**, *11*, 5982−5991.
(3) Gasteiger, H.; Panels, J.; Yan, S. Dependence of PEM fuel cell performance on catalyst loading. *J. Power Sources* **2004**, *127*, 162−171.
(4) Nie, Y.; Li, L.; Wei, Z. Recent advancements in Pt and Pt-free catalysts for oxygen reduction reaction. *Chem. Soc. Rev.* **2015**, *44*, 2168−2201.
(5) Stacy, J.; Regmi, Y. N.; Leonard, B.; Fan, M. The recent progress and future of oxygen reduction reaction catalysis: A review. *Renewable Sustainable Energy Rev.* **2017**, *69*, 401−414.
(6) Anastas, P.; Eghbali, N. Green chemistry: principles and practice. *Chem. Soc. Rev.* **2010**, *39*, 301−312.
(7) Asset, T.; Maillard, F.; Jaouen, F. *Supported Metal Single Atom Catalysis*; Serp, P., Pham Minh, D., Eds.; Wiley VCH: Weinheim, Germany, 2022; pp 531−582.
(8) Menga, D.; Low, J. L.; Li, Y.-S.; Arcon, I.; Koyuturk, B.; Wagner, F.; Ruiz-Zepeda, F.; Gaberscek, M.; Paulus, B.; Fellinger, T.-P. Resolving the dilemma of Fe−N−C catalysts by the selective synthesis of tetrapyrrolic active sites via an imprinting strategy. *J. Am. Chem. Soc.* **2021**, *143*, 18010−18019.
(9) Mehmood, A.; Gong, M.; Jaouen, F.; Roy, A.; Zitolo, A.; Khan, A.; Sougrati, M.-T.; Primbs, M.; Bonastre, A. M.; Fongalland, D.; et al. High loading of single atomic iron sites in Fe−NC oxygen reduction catalysts for proton exchange membrane fuel cells. *Nat. Catal.* **2022**, *5*, 311−323.
(10) Zhang, N.; Zhou, T.; Chen, M.; Feng, H.; Yuan, R.; Zhong, C.; Yan, W.; Tian, Y.; Wu, X.; Chu, W.; et al. High-purity pyrrole-type FeN_4 sites as a superior oxygen reduction electrocatalyst. *Energy Environ. Sci.* **2020**, *13*, 111−118.
(11) Luo, E.; Zhang, H.; Wang, X.; Gao, L.; Gong, L.; Zhao, T.; Jin, Z.; Ge, J.; Jiang, Z.; Liu, C.; et al. Single-atom Cr-N_4 sites designed for durable oxygen reduction catalysis in acid media. *Angew. Chem.* **2019**, *131*, 12599−12605.
(12) Liu, H.; Zhu, S.; Cui, Z.; Li, Z.; Wu, S.; Liang, Y. Unveiling the roles of multiple active sites during oxygen reduction reaction in Cr_2O_3@ Cr-NC composite catalyst. *J. Catal.* **2021**, *396*, 402−408.
(13) Parida, S. K.; Barik, T.; Jena, H. A polypyrrole derived nitrogen doped porous carbon support for an atomically dispersed Mn electrocatalyst for the oxygen reduction reaction. *Sustainable Energy Fuels* **2023**, *7*, 3684−3691.
(14) Di Liberto, G.; Pacchioni, G. Modeling Single-Atom Catalysis. *Adv. Mater.* **2023**, *35*, 2307150.
(15) Liu, K.; Fu, J.; Lin, Y.; Luo, T.; Ni, G.; Li, H.; Lin, Z.; Liu, M. Insights into the activity of single-atom Fe-NC catalysts for oxygen reduction reaction. *Nat. Commun.* **2022**, *13*, 2075.
(16) Rao, P.; Wu, D.; Wang, T.-J.; Li, J.; Deng, P.; Chen, Q.; Shen, Y.; Chen, Y.; Tian, X. Single atomic cobalt electrocatalyst for efficient oxygen reduction reaction. *eScience* **2022**, *2*, 399−404.
(17) Xu, H.; Wang, D.; Yang, P.; Liu, A.; Li, R.; Li, Y.; Xiao, L.; Zhang, J.; An, M. A theoretical study of atomically dispersed MN_4/C (M= Fe or Mn) as a high-activity catalyst for the oxygen reduction reaction. *Phys. Chem. Chem. Phys.* **2020**, *22*, 28297−28303.
(18) Tylus, U.; Jia, Q.; Strickland, K.; Ramaswamy, N.; Serov, A.; Atanassov, P.; Mukerjee, S. Elucidating oxygen reduction active sites in pyrolyzed metal−nitrogen coordinated non-precious-metal electrocatalyst systems. *J. Phys. Chem. C* **2014**, *118*, 8999−9008.
(19) Zitolo, A.; Goellner, V.; Armel, V.; Sougrati, M.-T.; Mineva, T.; Stievano, L.; Fonda, E.; Jaouen, F. Identification of catalytic sites for oxygen reduction in iron-and nitrogen-doped graphene materials. *Nat. Mater.* **2015**, *14*, 937−942.
(20) Hu, X.; Chen, S.; Chen, L.; Tian, Y.; Yao, S.; Lu, Z.; Zhang, X.; Zhou, Z. What is the Real Origin of the Activity of Fe−N−C Electrocatalysts in the O_2 Reduction Reaction? Critical Roles of Coordinating Pyrrolic N and Axially Adsorbing Species. *J. Am. Chem. Soc.* **2022**, *144*, 18144−18152.
(21) Ni, L.; Gallenkamp, C.; Wagner, S.; Bill, E.; Krewald, V.; Kramm, U. I. Identification of the catalytically dominant iron environment in iron-and nitrogen-doped carbon catalysts for the oxygen reduction reaction. *J. Am. Chem. Soc.* **2022**, *144*, 16827−16840.
(22) Chen, S.; Luo, T.; Li, X.; Chen, K.; Fu, J.; Liu, K.; Cai, C.; Wang, Q.; Li, H.; Chen, Y.; et al. Identification of the highly active Co−N_4 coordination motif for selective oxygen reduction to hydrogen peroxide. *J. Am. Chem. Soc.* **2022**, *144*, 14505−14516.
(23) Menga, D.; Guilherme Buzanich, A.; Wagner, F.; Fellinger, T.-P. Evaluation of the Specific Activity of M- N- Cs and the Intrinsic Activity of Tetrapyrrolic FeN_4 Sites for the Oxygen Reduction Reaction. *Angew. Chem., Int. Ed.* **2022**, *61*, No. e202207089.
(24) Calle-Vallejo, F.; Martínez, J. I.; Rossmeisl, J. Density functional studies of functionalized graphitic materials with late transition metals for oxygen reduction reactions. *Phys. Chem. Chem. Phys.* **2011**, *13*, 15639−15643.
(25) Calle-Vallejo, F.; Martínez, J.; García-Lastra, J.; Abad, E.; Koper, M. Oxygen reduction and evolution at single-metal active sites: Comparison between functionalized graphitic materials and proto-porphyrins. *Surf. Sci.* **2013**, *607*, 47−53.
(26) Low, J. L.; Paulus, B. Computational Modelling of Pyrrolic MN_4 Motifs Embedded in Graphene for Catalyst Design. *Catalysts* **2023**, *13*, 566.
(27) Barlocco, I.; Cipriano, L. A.; Di Liberto, G.; Pacchioni, G. Modeling hydrogen and oxygen evolution reactions on single atom catalysts with density functional theory: role of the functional. *Adv. Theory Simul.* **2023**, *6*, 2200513.
(28) Di Liberto, G.; Cipriano, L. A.; Pacchioni, G. Universal principles for the rational design of single atom electrocatalysts? Handle with care. *ACS Catal.* **2022**, *12*, 5846−5856.
(29) Zhou, F.; Cococcioni, M.; Marianetti, C. A.; Morgan, D.; Ceder, G. First-principles prediction of redox potentials in transition-metal compounds with LDA+ U. *Phys. Rev. B* **2004**, *70*, 235121.
(30) Wang, L.; Maxisch, T.; Ceder, G. Oxidation energies of transition metal oxides within the GGA+U framework. *Phys. Rev. B* **2006**, *73*, 195107.
(31) Patel, A. M.; Ringe, S.; Siahrostami, S.; Bajdich, M.; Nørskov, J. K.; Kulkarni, A. R. Theoretical approaches to describing the oxygen reduction reaction activity of single-atom catalysts. *J. Phys. Chem. C* **2018**, *122*, 29307−29318.
(32) Kirchhoff, B.; Ivanov, A.; Skúlason, E.; Jacob, T.; Fantauzzi, D.; Jónsson, H. Assessment of the accuracy of density functionals for calculating oxygen reduction reaction on nitrogen-doped graphene. *J. Chem. Theory Comput.* **2021**, *17*, 6405−6415.
(33) Khosravi, A.; Vessally, E.; Oftadeh, M.; Behjatmanesh-Ardakani, R. Ammonia capture by MN_4 (M= Fe and Ni) clusters embedded in graphene. *J. Coord. Chem.* **2018**, *71*, 3476−3486.
(34) Wang, K.; Huang, J.; Chen, H.; Wang, Y.; Song, S. Recent advances in electrochemical 2e oxygen reduction reaction for on-site hydrogen peroxide production and beyond. *Chem. Commun.* **2020**, *56*, 12109−12121.
(35) Zheng, R.; Meng, Q.; Zhang, L.; Ge, J.; Liu, C.; Xing, W.; Xiao, M. Co-based Catalysts for Selective H_2O_2 Electroproduction via 2-electron Oxygen Reduction Reaction. *Chem.—Eur. J.* **2023**, *29*, No. e202203180.
(36) Choi, C. H.; Lim, H.-K.; Chung, M. W.; Chon, G.; Ranjbar Sahraie, N.; Altin, A.; Sougrati, M.-T.; Stievano, L.; Oh, H. S.; Park, E. S.; et al. The Achilles' heel of iron-based catalysts during oxygen reduction in an acidic medium. *Energy Environ. Sci.* **2018**, *11*, 3176−3182.
(37) Bonakdarpour, A.; Lefevre, M.; Yang, R.; Jaouen, F.; Dahn, T.; Dodelet, J.-P.; Dahn, J. Impact of loading in RRDE experiments on Fe−N−C catalysts: two-or four-electron oxygen reduction? *Electrochem. Solid-State Lett.* **2008**, *11*, B105.
(38) Ramaswamy, N.; Mukerjee, S. Influence of inner-and outer-sphere electron transfer mechanisms during electrocatalysis of oxygen reduction in alkaline media. *J. Phys. Chem. C* **2011**, *115*, 18015−18026.

https://doi.org/10.1021/acs.jpcc.4c00299
J. Phys. Chem. C 2024, 128, 5075−5083

(39) Malko, D.; Kucernak, A. Kinetic isotope effect in the oxygen reduction reaction (ORR) over Fe-N/C catalysts under acidic and alkaline conditions. *Electrochem. Commun.* **2017**, *83*, 67−71.
(40) Ramaswamy, N.; Tylus, U.; Jia, Q.; Mukerjee, S. Activity descriptor identification for oxygen reduction on nonprecious electrocatalysts: linking surface science to coordination chemistry. *J. Am. Chem. Soc.* **2013**, *135*, 15443−15449.
(41) Ahlrichs, R.; Bär, M.; Häser, M.; Horn, H.; Kölmel, C. Electronic structure calculations on workstation computers: The program system turbomole. *Chem. Phys. Lett.* **1989**, *162*, 165−169.
(42) Perdew, J. P.; Ernzerhof, M.; Burke, K. Rationale for mixing exact exchange with density functional approximations. *J. Chem. Phys.* **1996**, *105*, 9982−9985.
(43) Ernzerhof, M.; Scuseria, G. E. Assessment of the Perdew−Burke−Ernzerhof exchange-correlation functional. *J. Chem. Phys.* **1999**, *110*, 5029−5036.
(44) Grimme, S.; Antony, J.; Ehrlich, S.; Krieg, H. A consistent and accurate ab initio parametrization of density functional dispersion correction (DFT-D) for the 94 elements H-Pu. *J. Chem. Phys.* **2010**, *132*, 154104.
(45) Grimme, S.; Ehrlich, S.; Goerigk, L. Effect of the damping function in dispersion corrected density functional theory. *J. Comput. Chem.* **2011**, *32*, 1456−1465.
(46) Weigend, F.; Ahlrichs, R. Balanced basis sets of split valence, triple zeta valence and quadruple zeta valence quality for H to Rn: Design and assessment of accuracy. *Phys. Chem. Chem. Phys.* **2005**, *7*, 3297−3305.
(47) Klamt, A.; Schüürmann, G. COSMO: a new approach to dielectric screening in solvents with explicit expressions for the screening energy and its gradient. *J. Chem. Soc., Perkin Trans. 2* **1993**, *2*, 799−805.
(48) Reed, A. E.; Weinstock, R. B.; Weinhold, F. Natural population analysis. *J. Chem. Phys.* **1985**, *83*, 735−746.
(49) Momma, K.; Izumi, F. VESTA 3 for three-dimensional visualization of crystal, volumetric and morphology data. *J. Appl. Crystallogr.* **2011**, *44*, 1272−1276.
(50) Nørskov, J. K.; Rossmeisl, J.; Logadottir, A.; Lindqvist, L.; Kitchin, J. R.; Bligaard, T.; Jonsson, H. Origin of the overpotential for oxygen reduction at a fuel-cell cathode. *J. Phys. Chem. B* **2004**, *108*, 17886−17892.
(51) Chase, M. W.; National Institute of Standards and Technology (US) *NIST-JANAF thermochemical tables*; American Chemical Society: Washington, DC, 1998; Vol. *9*.
(52) Mehmood, A.; Pampel, J.; Ali, G.; Ha, H. Y.; Ruiz-Zepeda, F.; Fellinger, T.-P. Facile metal coordination of active site imprinted nitrogen doped carbons for the conservative preparation of non-noble metal oxygen reduction electrocatalysts. *Adv. Energy Mater.* **2018**, *8*, 1701771.
(53) Sabatier, P. La catalyse en chimie organique. *Encyclopédie de science chimique appliquée aux arts industriels*; Read Books, 1920; pub. sous la direction de C. Chabrié; C. Béranger.
(54) Ooka, H.; Huang, J.; Exner, K. S. The sabatier principle in electrocatalysis: Basics, limitations, and extensions. *Front. Energy res.* **2021**, *9*, 654460.
(55) Karmodak, N.; Nørskov, J. K. Activity And Stability of Single-And Di-Atom Catalysts for the O_2 Reduction Reaction. *Angew. Chem.* **2023**, *135*, No. e202311113.
(56) Tang, C.; Chen, L.; Li, H.; Li, L.; Jiao, Y.; Zheng, Y.; Xu, H.; Davey, K.; Qiao, S.-Z. Tailoring acidic oxygen reduction selectivity on single-atom catalysts via modification of first and second coordination spheres. *J. Am. Chem. Soc.* **2021**, *143*, 7819−7827.
(57) Bi, P.; Xiao, T.; Yang, X.; Niu, M.; Wen, Z.; Zhang, K.; Qin, W.; So, S. K.; Lu, G.; Hao, X.; et al. Regulating the vertical phase distribution by fullerene-derivative in high performance ternary organic solar cells. *Nano Energy* **2018**, *46*, 81−90.
(58) Choi, C. H.; Lim, H.-K.; Chung, M. W.; Park, J. C.; Shin, H.; Kim, H.; Woo, S. I. Long-range electron transfer over graphene-based catalyst for high-performing oxygen reduction reactions: importance of size, N-doping, and metallic impurities. *J. Am. Chem. Soc.* **2014**, *136*, 9070−9077.
(59) Jung, E.; Shin, H.; Lee, B.-H.; Efremov, V.; Lee, S.; Lee, H. S.; Kim, J.; Hooch Antink, W.; Park, S.; Lee, K.-S.; et al. Atomic-level tuning of Co−N−C catalyst for high-performance electrochemical H_2O_2 production. *Nat. Mater.* **2020**, *19*, 436−442.
(60) Amiinu, I. S.; Liu, X.; Pu, Z.; Li, W.; Li, Q.; Zhang, J.; Tang, H.; Zhang, H.; Mu, S. From 3D ZIF nanocrystals to Co−N_x/C nanorod array electrocatalysts for ORR, OER, and Zn−air batteries. *Adv. Funct. Mater.* **2018**, *28*, 1704638.
(61) Xu, H.; Wang, D.; Yang, P.; Liu, A.; Li, R.; Li, Y.; Xiao, L.; Ren, X.; Zhang, J.; An, M. Atomically dispersed M−N−C catalysts for the oxygen reduction reaction. *J. Mater. Chem. A* **2020**, *8*, 23187−23201.
(62) Sun, Y.; Silvioli, L.; Sahraie, N. R.; Ju, W.; Li, J.; Zitolo, A.; Li, S.; Bagger, A.; Arnarson, L.; Wang, X.; et al. Activity−Selectivity Trends in the Electrochemical Production of Hydrogen Peroxide over Single-Site Metal−Nitrogen−Carbon Catalysts. *J. Am. Chem. Soc.* **2019**, *141*, 12372−12381.
(63) Ku, Y.-P.; Ehelebe, K.; Hutzler, A.; Bierling, M.; Bohm, T.; Zitolo, A.; Vorokhta, M.; Bibent, N.; Speck, F. D.; Seeberger, D.; et al. Oxygen Reduction Reaction in Alkaline Media Causes Iron Leaching from Fe−N−C Electrocatalysts. *J. Am. Chem. Soc.* **2022**, *144*, 9753−9763.
(64) Fan, X.; Gao, Y.; Yang, F.; Low, J. L.; Wang, L.; Paulus, B.; Wang, Y.; Trampuz, A.; Cheng, C.; Haag, R. A Copper Single-Atom Cascade Bionanocatalyst for Treating Multidrug-Resistant Bacterial Diabetic Ulcer. *Adv. Funct. Mater.* **2023**, *33*, 2301986.
(65) Jaouen, F.; Charreteur, F.; Dodelet, J. Fe-based catalysts for oxygen reduction in PEMFCs: Importance of the disordered phase of the carbon support. *J. Electrochem. Soc.* **2006**, *153*, A689.
(66) Lefèvre, M.; Dodelet, J.-P. Fe-based catalysts for the reduction of oxygen in polymer electrolyte membrane fuel cell conditions: determination of the amount of peroxide released during electro-reduction and its influence on the stability of the catalysts. *Electrochim. Acta* **2003**, *48*, 2749−2760.
(67) Goellner, V.; Armel, V.; Zitolo, A.; Fonda, E.; Jaouen, F. Degradation by hydrogen peroxide of metal-nitrogen-carbon catalysts for oxygen reduction. *J. Electrochem. Soc.* **2015**, *162*, H403−H414.
(68) Bae, G.; Chung, M. W.; Ji, S. G.; Jaouen, F.; Choi, C. H. pH effect on the H_2O_2-induced deactivation of Fe-NC catalysts. *ACS Catal.* **2020**, *10*, 8485−8495.

https://doi.org/10.1021/acs.jpcc.4c00299
J. Phys. Chem. C 2024, 128, 5075−5083